2013 IEEE International Conference on Robotics and Automation (ICRA)
Karlsruhe, Germany, May 6-10, 2013

Pre- and Post-Grasping Robot Motion Planning To Capture and Stabilize a Tumbling/Drifting Free-Floater with Uncertain Dynamics

Farhad Aghili

Abstract— **This paper focuses on optimal and seamless guidance of robotic manipulators, in both pre- and post-grasp phases, to capture and stabilize a tumbling and drifting free-floating object. All dynamics parameters of the object are assumed to be unknown with the exception its mass and the trace of the inertia matrix. In the pre-grasping phase, an optimal trajectory is planned to intercept a grasping point on the target with zero relative velocity subject to acceleration limit and adequate target alignment while minimizing the fly time and/or distance. In the post-grasping phase, the manipulator damps out the targets's angular and linear momentums as quickly as possible subject to the constraint that the magnitude of the exerted force and torque remain below their pre-specified values. The unknown parameters in addition to the relative linear and angular velocities of the target needed for the motion planning are estimated by a Kalman filter estimator. Finally, an end-to-end validation of the robotic operation for grasping and stabilizing a tumbling/drifting free-floating object using the proposed robot motion planning scheme is presented by combination of experimental and simulation results.**

I. Introduction

In the past two decades, several on-orbit servicing missions using a space manipulator have been proposed not only for repairing, rescuing, and refueling failed satellites [1] but also for removal of defunct satellites or large orbital debris [2]. Robotic manipulators can be operated from ground or autonomously depending on mission constraints, requirements, and the level of technology readiness. Nevertheless, increased autonomy for robotic systems for on-orbit servicing missions is identified as the key technology by many space agencies [3]. One of the autonomous capability often needed for these missions is for robotic capturing of a tumbling space object.

Orbital debris is defined as the collection of man-made objects in space whose size may range from small pieces released during satellite deployment to massive defunct satellites and rocket bodies. Despite all orbital debits eventually reenter the Earth atmosphere within few years or centuries, depending on their size and orbit, space debris is on the rise owing to the increasing rate of satellite launches and retirements [4]. Nowadays the international concern is that the population growth has reached an unstable point in some congested orbits such that the collision between orbital debris objects could cause a cascade scenario–the Kessler syndrome [5]. Based on Inter Agency Debris Coordination (IADC) recommendations, the space environment can be stabilized and preserved upon continual removal of large orbital debris objects. A comprehensive concept for active orbital debris removal (ODR) system makes use of a servicing spacecraft equipped with a robotic system with grappling device on it [6], [7]. Since orbital debris objects do not have a functional attitude control system, it is common for them to tumble. Ground observations also reveal that many space debris objects do have tumbling motion indeed [2]. Experiments conducted on ISS revealed that, in the presence of command latency, even a trained operator cannot successfully capture a free-floater unless the angular rate is extremely low. In fact, although several missions for free-flyer capture using a robotic arm on-orbit have been demonstrated so far [1], [8]–[10], robotic capturing of a tumbling satellite has not been attempted yet.

It was shown that nearly any control schemes that can be used for fixed-base manipulators can be also implemented on free-floating space robot, provided that the platform attitude and position are estimated and then taken into account [11], [12]. However, guidance of a robotic manipulator in order to rendezvous and capture a tumbling free-floating object in a safe and secure manner remains a challenging task still [13]. A majority of the techniques developed for the real-time motion planning and the robotic interception of a moving target assume a *point mass* target [14]–[16]. Interception of a spinning or tumbling satellite is a more difficult task due to the complex dynamics of rotating rigid bodies [17].

This paper presents pre-grasping and post-grasping motion planning schemes for autonomous robotic capture and stabilization of a tumbling space object using vision feedback. First, an adaptive Kalman filter gives estimations of the motion states and the dynamics parameters of the free-floating target from noisy measurements of a laser camera system. Subsequently, the estimated states are used to plan the trajectory of the robot's end-effector in the pre-grasping and post-grasping phases. In the pre-grasping phase, the robot motion to intercept the object in minimum time is planned subject to robot acceleration limit and the following constrains at the time of interception: i) the robot's end-effector and the target's grapple fixture have zero relative velocity therefore the capture is with minimum impact; ii) the target object is adequately aligned and becomes accessible for robotic grasping. In the post-grasping phase, when the end-effector mechanically connects to the target, the manipulator stabilizes the drifting and tumbling target satellite as quickly as possible without applying excessive force and torque. Finally experimental results obtained from a hardware-in-the-loop simulation are presented.

F. Aghili is a research scientist with the Space Exploration directory of the Canadian Space Agency (CSA), Saint-Hubert, Quebec J3Y 8Y9, Canada, farhad.aghili@asc-csa.gc.ca. He is also an Affiliate Associate professor at Concordia University.

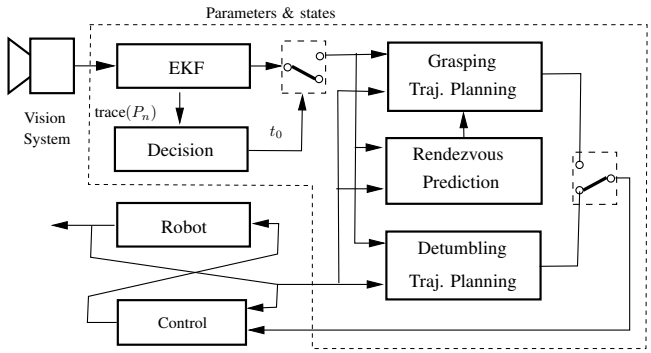

Fig. 1. The concept of robotic capturing and passivation of a tumbling satellite

II. Target Motion and Parameters Estimation

The implementation of optimal motion-planning trajectories, which will be later described in the next sections, requires the values of the full motion states as well as the dynamic parameters of the target. Since the vision system gives only measurement of the object pose, we need to estimate the rest of variables. This section describes an extended EKF-based estimator to estimate not only the system states but also all the relevant parameters.

Fig. II illustrates a robot trying to capture a drifting and tumbling object. $\{\mathcal{A}\}$ is assumed the inertial frame, while coordinate frame $\{\mathcal{B}\}$ is attached to the body of the target. Coordinate frame $\{\mathcal{C}\}$ is fixed to the target's grapple fixture located at $\boldsymbol{\varrho}$ from the origin of $\{\mathcal{B}\}$; it is the pose of $\{\mathcal{C}\}$ which is measured by the vision system. We further assume that the target tumbles with angular velocity $\boldsymbol{\omega}$. Since it is not possible to identify the absolute values of the inertia parameters from observations of torque-free tumbling motion [17], we use the following non-dimensional inertia parameters

$$\sigma_x = \frac{I_{yy} - I_{zz}}{I_{xx}}, \quad \sigma_y = \frac{I_{zz} - I_{xx}}{I_{yy}}, \quad \sigma_z = \frac{I_{xx} - I_{yy}}{I_{zz}} \tag{1}$$

where I_{xx}, I_{yy}, and I_{zz} denote the target's principal moments of inertia, and $\boldsymbol{I}_c = \mathrm{diag}(I_{xx}, I_{yy}, I_{zz})$ is the corresponding inertia tensor. Notice that the dimensionless inertia parameters are bounded between -1 and 1, i.e.,

$$-1 < \sigma_x, \sigma_y, \sigma_z < 1$$

Furthermore, the parameters are not independent as they are mutually related by the following identities

$$\sigma_x = -\frac{\sigma_y + \sigma_z}{1 + \sigma_y\sigma_z}, \quad \sigma_y = -\frac{\sigma_x + \sigma_z}{1 + \sigma_x\sigma_z}, \quad \sigma_z = -\frac{\sigma_y + \sigma_x}{1 + \sigma_y\sigma_x}$$

Then, the Euler's equations can be expressed in terms of any set of independent dimensionless inertia parameters, say $\boldsymbol{\sigma} = [\sigma_x \ \sigma_y]^T$, as

$$\dot{\boldsymbol{\omega}} = \boldsymbol{d}(\boldsymbol{\omega}, \boldsymbol{\sigma}) + \boldsymbol{B}(\boldsymbol{\sigma})\boldsymbol{\epsilon}_\tau \tag{2}$$

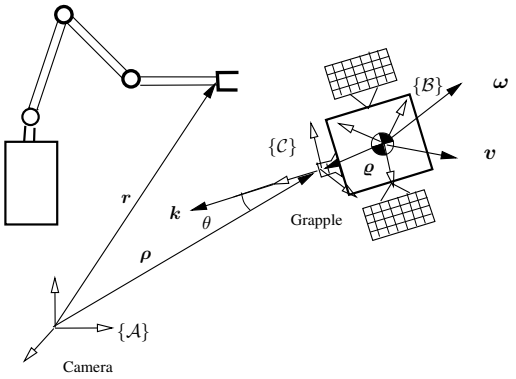

(a) Pre-grasping phase

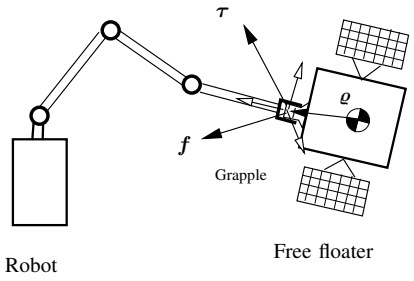

(b) Post-grasping phase

where

$$\boldsymbol{B}(\boldsymbol{\sigma}) = \mathbf{1}_3 + \begin{bmatrix} \frac{2+\sigma_y-\sigma_z}{1+\sigma_y\sigma_z} & 0 & 0 \\ 0 & \frac{2+\sigma_z-\sigma_x}{1+\sigma_x\sigma_z} & 0 \\ 0 & 0 & \frac{2+\sigma_x-\sigma_y}{1+\sigma_x\sigma_y} \end{bmatrix},$$

$$\boldsymbol{d}(\boldsymbol{\omega}, \boldsymbol{\sigma}) = \begin{bmatrix} \sigma_x\omega_y\omega_z \\ \sigma_y\omega_x\omega_z \\ \sigma_z\omega_x\omega_y \end{bmatrix}, \quad \text{and}$$

$$\boldsymbol{\epsilon}_\tau = \frac{\boldsymbol{\tau}}{\mathrm{tr}(\boldsymbol{I}_c)}$$

is defined as the acceleration disturbance with $\mathrm{tr}(\cdot)$ denoting the trace of a matrix.

Let quaternion $\boldsymbol{q} = [\boldsymbol{q}_v^T \ q_o]^T$ represent the orientation of the target. Then, the time derivative of the quaternion can be expressed by

$$\dot{\boldsymbol{q}} = \frac{1}{2}\boldsymbol{\Omega}(\boldsymbol{\omega})\boldsymbol{q} \quad \text{where} \quad \boldsymbol{\Omega}(\boldsymbol{\omega}) = \begin{bmatrix} -[\boldsymbol{\omega}\times] & \boldsymbol{\omega} \\ -\boldsymbol{\omega}^T & 0 \end{bmatrix} \tag{3}$$

Coincidentally, the matrix function $\boldsymbol{\Omega}(\cdot)$ also appears in the quaternion product

$$\boldsymbol{q}\otimes \triangleq q_0\mathbf{1}_4 + \boldsymbol{\Omega}(\boldsymbol{q}_v) \tag{4}$$

The translational motion of the target can be simply expressed by

$$\ddot{\boldsymbol{\rho}}_o = \boldsymbol{\epsilon}_f \tag{5}$$

where $\boldsymbol{\rho}_o$ denotes the location of the target CM expressed in the inertial frame $\{\mathcal{A}\}$, and $\boldsymbol{\epsilon}_f$ is the disturbance force per unit mass. Consider the state vector to be estimated by KF as

$$\boldsymbol{x} = [\boldsymbol{q}_v^T \ \boldsymbol{\omega}^T \ \boldsymbol{\rho}_o^T \ \dot{\boldsymbol{\rho}}_o{}^T \ \boldsymbol{\sigma}^T \ \boldsymbol{\varrho}^T \ \boldsymbol{\mu}_v^T]^T \tag{6}$$

where $\boldsymbol{\varrho}$ is the location of target's center of mass and $\boldsymbol{\mu}$ is a unit quaternion representing the orientation of the principal axes, i.e., orientation of $\{\mathcal{B}\}$ w.r.t. $\{\mathcal{C}\}$. Now, assume that the dynamics parameters of the target $\boldsymbol{\sigma}$, $\boldsymbol{\varrho}$, and $\boldsymbol{\eta}$ remain constant, the process dynamics including (2), (3), and (5) can be described in this compact form

$$\dot{\boldsymbol{x}} = \boldsymbol{\gamma}(\boldsymbol{x}) + \boldsymbol{G}(\boldsymbol{x})\boldsymbol{\epsilon}, \tag{7}$$

where

$$\boldsymbol{G}(\boldsymbol{x}) = \begin{bmatrix} \mathbf{0}_3 & \mathbf{0}_3 \\ \boldsymbol{B}(\boldsymbol{\sigma}) & \mathbf{0}_3 \\ \mathbf{0}_3 & \mathbf{0}_3 \\ \mathbf{0}_3 & \mathbf{1}_3 \\ \mathbf{0}_{8\times 3} & \mathbf{0}_{8\times 3} \end{bmatrix} \quad \text{and} \quad \boldsymbol{\epsilon} = \begin{bmatrix} \boldsymbol{\epsilon}_\tau \\ \boldsymbol{\epsilon}_f \end{bmatrix}$$

Here, $\boldsymbol{\epsilon}$ is assumed to be white noise with covariance $E[\boldsymbol{\epsilon}\boldsymbol{\epsilon}^T] = \boldsymbol{Q}$. Linearization of the nonlinear vector function in (7) about the estimated states, which is needed to be used for the covariance propagation of extended Kalman filter, i.e. $\boldsymbol{\Gamma} = \big(\partial\boldsymbol{\gamma}(\boldsymbol{x})/\partial\boldsymbol{x}\big)_{\boldsymbol{x}=\hat{\boldsymbol{x}}}$, can be derived as

$$\boldsymbol{\Gamma} = \begin{bmatrix} -[\hat{\boldsymbol{\omega}}\times] & \frac{1}{2}\mathbf{1}_3 & \mathbf{0}_3 & \mathbf{0}_3 & \mathbf{0}_{3\times 2} & \mathbf{0}_{3\times 6} \\ \mathbf{0}_3 & \boldsymbol{M} & \mathbf{0}_3 & \mathbf{0}_3 & \boldsymbol{N} & \mathbf{0}_{3\times 6} \\ \mathbf{0}_3 & \mathbf{0}_3 & \mathbf{0}_3 & \mathbf{1}_3 & \mathbf{0}_{3\times 2} & \mathbf{0}_{3\times 6} \\ \mathbf{0}_{11\times 3} & \mathbf{0}_{11\times 3} & \mathbf{0}_{11\times 3} & \mathbf{0}_{11\times 3} & \mathbf{0}_{11\times 2} & \mathbf{0}_{11\times 6} \end{bmatrix} \tag{8}$$

where

$$\boldsymbol{M} = \frac{\partial \boldsymbol{d}}{\partial \boldsymbol{\omega}}\Big|_{\hat{\boldsymbol{\omega}},\hat{\boldsymbol{\sigma}}} = \begin{bmatrix} 0 & \hat{\sigma}_x\hat{\omega}_z & \hat{\sigma}_x\hat{\omega}_y \\ \hat{p}_y\hat{\omega}_z & 0 & \hat{\sigma}_y\hat{\omega}_x \\ \hat{\sigma}_z\hat{\omega}_y & \hat{\sigma}_z\hat{\omega}_x & 0 \end{bmatrix}$$

$$\boldsymbol{N} = \frac{\partial \boldsymbol{d}}{\partial \boldsymbol{\sigma}}\Big|_{\hat{\boldsymbol{\omega}},\hat{\boldsymbol{\sigma}}} = \begin{bmatrix} \hat{\omega}_y\hat{\omega}_z & 0 \\ 0 & \hat{\omega}_x\hat{\omega}_z \\ \frac{\hat{\sigma}_y^2-1}{(1+\hat{\sigma}_x\hat{\sigma}_y)^2}\hat{\omega}_x\hat{\omega}_y & \frac{\hat{\sigma}_x^2-1}{(1+\hat{\sigma}_x\hat{\sigma}_y)^2}\hat{\omega}_x\hat{\omega}_y \end{bmatrix}$$

Suppose that the vision system gives a noisy measurement of the position and orientation of coordinate $\{\mathcal{C}\}$ attached to the grapple fixture with respect to the inertial coordinate system $\{\mathcal{A}\}$; see Fig. II. Denoting the orientation of $\{\mathcal{C}\}$ with respect to $\{\mathcal{A}\}$ by unit quaternion $\boldsymbol{\eta}$, one can write the measurement vector as

$$\boldsymbol{z} = \begin{bmatrix} \boldsymbol{\rho} \\ \boldsymbol{\eta} \end{bmatrix} + \boldsymbol{v} \tag{9}$$

where the position and orientation are represented by vector $\boldsymbol{\rho}$ and unit quaternion $\boldsymbol{\eta}$, and $\boldsymbol{v}$ is the measurement noise with covariance $\boldsymbol{R} = E[\boldsymbol{v}\boldsymbol{v}^T]$. The orientation of the principal axes is not a priori known and so is not the alignment of coordinate frame $\{\mathcal{C}\}$ with respect to $\{\mathcal{B}\}$. The quaternion $\boldsymbol{\eta}$ can be considered as two successive orientations as

$$\boldsymbol{\eta} = \boldsymbol{\mu} \otimes \boldsymbol{q}. \tag{10}$$

where $\boldsymbol{\mu}$ represents the orientation of the principal axes. Then, the observation equations can be written as a nonlinear function of the states

$$\boldsymbol{z} = \boldsymbol{h}(\boldsymbol{x}) + \boldsymbol{v} \quad \text{where} \quad \boldsymbol{h}(\boldsymbol{x}) = \begin{bmatrix} \boldsymbol{\rho}_o + \boldsymbol{A}(\boldsymbol{q})\boldsymbol{\varrho} \\ \boldsymbol{\mu} \otimes \boldsymbol{q} \end{bmatrix} \tag{11}$$

where

$$\boldsymbol{A}(\boldsymbol{q}) = (2q_o^2 - 1)\mathbf{1}_3 + 2q_o[\boldsymbol{q}_v\times] + 2\boldsymbol{q}_v\boldsymbol{q}_v^T \tag{12}$$

is the corresponding rotation matrix. The observation sensitivity matrix $\boldsymbol{H} = \big(\partial\boldsymbol{h}(\boldsymbol{x})/\partial\boldsymbol{x}\big)_{\boldsymbol{x}=\hat{\boldsymbol{x}}}$ can be obtained as

$$\boldsymbol{H} = \begin{bmatrix} -2\boldsymbol{A}(\hat{\boldsymbol{q}})[\hat{\boldsymbol{\varrho}}\times] & \mathbf{0}_{3\times 3} & \mathbf{1}_3 & \mathbf{0}_{3\times 5} & \boldsymbol{A}(\hat{\boldsymbol{q}}) & \mathbf{0}_{3\times 3} \\ \boldsymbol{\Upsilon}(\hat{\boldsymbol{q}},\hat{\boldsymbol{\mu}}) & \mathbf{0}_{4\times 3} & \mathbf{0}_{4\times 3} & \mathbf{0}_{4\times 5} & \mathbf{0}_{4\times 3} & \boldsymbol{\Upsilon}(\hat{\boldsymbol{q}},\hat{\boldsymbol{\mu}}) \end{bmatrix} \tag{13}$$

where

$$\boldsymbol{\Upsilon} = \begin{bmatrix} \hat{q}_o\hat{\eta}_o\mathbf{1}_3 - \hat{q}_o[\hat{\boldsymbol{\mu}}_v\times] + \hat{\eta}_o[\hat{\boldsymbol{q}}_v\times] - [\hat{\boldsymbol{q}}_v\times][\hat{\boldsymbol{\mu}}_v\times] - \hat{\boldsymbol{q}}_v\hat{\boldsymbol{\mu}}_v^T \\ (\hat{\boldsymbol{q}}_v \times \hat{\boldsymbol{\mu}}_v)^T - \hat{\eta}_o\hat{\boldsymbol{q}}_v^T - \hat{q}_o\hat{\boldsymbol{\mu}}_v^T \end{bmatrix}.$$

Now, one can design an extended Kalman filter (EKF) based on the derived linearized models (8) and (13).

III. Pre-Grasping Trajectory Planning & Rendezvous

A. Motion Planning

Let $\boldsymbol{r}$ represent the position of the robot's end-effector expressed in the inertial frame. In the pre-capturing phase, the main objective is to bring the end-effector from its initial position $\boldsymbol{r}_o$ at initial time $t = t_o$ to a grasping location along the trajectory of the grapple fixture with zero relative velocity while satisfying the acceleration magnitude being less than $a_{\max}$. That is,

$$\|\ddot{\boldsymbol{r}}(t)\| \le a_{\max} \qquad \forall t \in [t_o \;\; t_f) \tag{14}$$

$$\boldsymbol{r}(t_f) = \boldsymbol{\rho}(t_f) \quad \text{and} \quad \dot{\boldsymbol{r}}(t_f) = \dot{\boldsymbol{\rho}}(t_f). \tag{15}$$

Now, assume that the optimal trajectory is generated by the following second order system

$$\ddot{\boldsymbol{r}} = \boldsymbol{u} \tag{16}$$

In order to avoid introduction of new variables, let us redefine vector $\boldsymbol{x}$ to be the state vector of the entire system

$$\boldsymbol{x} = [\boldsymbol{s}^T \; \boldsymbol{r}^T \; \dot{\boldsymbol{r}}^T]^T, \quad \text{where} \quad \boldsymbol{s} = [\boldsymbol{q}^T \; \boldsymbol{\omega}^T \; \boldsymbol{\rho}_o^T]^T$$

being the states of the target. Then, combining (2), (3), and (16), we get the following autonomous system

$$\dot{\boldsymbol{x}}(\boldsymbol{x},\boldsymbol{u}) = \begin{bmatrix} \frac{1}{2}\boldsymbol{\Omega}(\boldsymbol{\omega})\boldsymbol{q} \\ \boldsymbol{d}(\boldsymbol{\omega}) \\ \dot{\boldsymbol{\rho}}_o \\ \dot{\boldsymbol{r}} \\ \boldsymbol{u} \end{bmatrix}, \tag{17}$$

and $\dot{\boldsymbol{\rho}}_o$ is constant. Notice that the target location and velocity can be computed from the state vector by

$$\boldsymbol{\rho}(\boldsymbol{x}) = \boldsymbol{\rho}_o + \boldsymbol{A}(\boldsymbol{q})\boldsymbol{\varrho} \tag{18a}$$

$$\dot{\boldsymbol{\rho}}(\boldsymbol{x}) = \dot{\boldsymbol{\rho}}_o + \boldsymbol{A}(\boldsymbol{q})(\boldsymbol{\omega} \times \boldsymbol{\varrho}). \tag{18b}$$

In the following analysis, an optimal solution to the input $\boldsymbol{u}$ of system (17) is sought to minimize the following cost function

$$J = \phi(\boldsymbol{x}_f) + \int_{t_o}^{t_f} 1 + c(\boldsymbol{u})d\tau, \tag{19}$$

where $\boldsymbol{x}_f = \boldsymbol{x}(t_f)$ and

$$c(\boldsymbol{u}) = \begin{cases} \kappa(\|\boldsymbol{u}\|^2 - a_{\max}^2) & \text{if} \quad \|\boldsymbol{u}\| \geq a_{\max} \\ 0 & \text{otherwise} \end{cases} \tag{20}$$

is a penalty function, subject to the following terminal state constraint

$$\boldsymbol{\psi}[\boldsymbol{x}(t_f)] = \boldsymbol{0} \qquad \text{where} \qquad \boldsymbol{\psi}(\boldsymbol{x}) = \begin{bmatrix} \boldsymbol{\rho}(\boldsymbol{x}) - \boldsymbol{r} \\ \dot{\boldsymbol{\rho}}(\boldsymbol{x}) - \dot{\boldsymbol{r}} \end{bmatrix}, \tag{21}$$

The "soft constraint" (20) with very large penalty becomes equivalent to the "hard constraint" (14). Therefore, the time of travel t_f is minimized if the nonintegral part of the cost function (19) is set to zero. However, function $\phi(\boldsymbol{x}_f)$ is added to satisfy some capture conditions as follows. In order to gauge the accessibility of the grapple fixture by the robot, let us define the line of sight angle θ that is made by the opposite direction of vector $\boldsymbol{r}$ (at the time of interception) and unit vector $\boldsymbol{k}$ attached to the grapple fixture; see Fig. 2(a). It is assumed that vector $\boldsymbol{k}$ is expressed in the target frame $\{\mathcal{C}\}$ in such a way that $\theta = 0$ corresponds to the most suitable object alignment for robotic grasping and conversely the grasping is not possible when $\theta = \pi$. Therefore, the non-integral part of the cost function (19) is set to

$$\begin{aligned} \phi(\boldsymbol{x}) &= w_1 \|\boldsymbol{r}\| - w_2 \cos\theta \\ &= \frac{w_1 \|\boldsymbol{r}\|^2 + w_2 \boldsymbol{r}^T \boldsymbol{A}(\boldsymbol{q}) \boldsymbol{k}}{\|\boldsymbol{r}\|} \end{aligned} \tag{22}$$

where $w_1 > 0$ and $w_2 > 0$ are scaler weights. Clearly, the incorporation of ϕ in the cost function tends to minimize the distance $\|\boldsymbol{r}(t_f)\|$ and the line-of-sight angle $\theta(t_f)$.

The Hamiltonian for system (17) and (19) can be written as

$$\mathcal{H} = 1 + c(\boldsymbol{u}) + \boldsymbol{\lambda}^T \dot{\boldsymbol{x}}(\boldsymbol{x}, \boldsymbol{u}) \tag{23}$$

According to the optimal control theory [18], the costate and optimal input, $\boldsymbol{u}^*$, must satisfy the following partial derivatives:

$$\dot{\boldsymbol{\lambda}} = -\frac{\partial \mathcal{H}}{\partial \boldsymbol{x}}, \qquad \frac{\partial \mathcal{H}}{\partial \boldsymbol{u}} = \boldsymbol{0}. \tag{24}$$

Splitting the vector of costate as $\boldsymbol{\lambda} = [\boldsymbol{\lambda}_s^T \ \boldsymbol{\lambda}_r^T \ \boldsymbol{\lambda}_u^T]^T$, where $\boldsymbol{\lambda}_s \in \mathbb{R}^9$ and $\boldsymbol{\lambda}_r, \boldsymbol{\lambda}_u \in \mathbb{R}^3$, and the applying (24) to our Hamiltonian (23) yields the following identities

$$\dot{\boldsymbol{\lambda}}_r = \boldsymbol{0} \tag{25a}$$

$$\dot{\boldsymbol{\lambda}}_u = -\boldsymbol{\lambda}_r \tag{25b}$$

$$\boldsymbol{\lambda}_u = -2\kappa \boldsymbol{u}^* \tag{25c}$$

One can readily infer from (25a)–(25c) that the expression of the acceleration trajectory is:

$$\boldsymbol{u}^* = \boldsymbol{c}_1 (t - t_o) + \boldsymbol{c}_2, \tag{26}$$

where $\boldsymbol{c}_1$ and $\boldsymbol{c}_2$ are defined such that

$$\begin{aligned} \boldsymbol{\lambda}_r &= 2\kappa \boldsymbol{c}_1 \\ \boldsymbol{\lambda}_u &= -2\kappa \boldsymbol{c}_1 (t - t_o) - 2\kappa \boldsymbol{c}_2 \end{aligned} \tag{27}$$

Subsequently, one can obtain the position and velocity trajectories via integration. The constant polynomial coefficients $\boldsymbol{c}_1$ and $\boldsymbol{c}_2$ are solved by imposing the initial and terminal conditions, i.e.,

$$\begin{aligned} \boldsymbol{c}_1 &= \frac{6\big(\dot{\boldsymbol{\rho}}(t_f) + \dot{\boldsymbol{r}}_r(t_o)\big)}{(t_f - t_o)^2} - \frac{12\big(\boldsymbol{\rho}(t_f) - \boldsymbol{r}(t_o)\big)}{(t_f - t_o)^3} \\ \boldsymbol{c}_2 &= -\frac{2\big(\dot{\boldsymbol{\rho}}(t_f) + 2\dot{\boldsymbol{r}}(t_o)\big)}{t_f - t_o} + \frac{6\big(\boldsymbol{\rho}(t_f) - \boldsymbol{r}(t_o)\big)}{(t_f - t_o)^2} \end{aligned} \tag{28}$$

In view of (26) and (28), the expression of the optimal control input can be written as a function of initial time, t_o, and current time, t, in this form

$$\begin{aligned} \boldsymbol{u}^*(t_o, t) =& \frac{-12t + 6t_o + 6t_f}{(t_f - t_o)^3} \big(\boldsymbol{\rho}(t_f) - \boldsymbol{r}(t)\big) \\ &+ \frac{6t - 4t_o - 2t_f}{(t_f - t_o)^2} \big(\dot{\boldsymbol{\rho}}(t_f) - \dot{\boldsymbol{r}}(t)\big) \\ &+ \frac{12t - 6t_o - 6t_f}{(t_f - t_o)^2} \dot{\boldsymbol{\rho}}(t_f) \end{aligned} \tag{29}$$

Now, the control input at any given time $t \in [t_o, t_f)$ can be also calculated by setting the values of the position and velocity at that time as the initial values. Therefore, by setting the floating initial time $t_o = t$ in (29), we will arrive at the optimal acceleration trajectory $\ddot{\boldsymbol{r}}^*(t) = \boldsymbol{u}^*(t, t)$ as

$$\begin{aligned} \ddot{\boldsymbol{r}}^*(t) =& \frac{6}{(t_f - t)^2} \big(\boldsymbol{\rho}(t_f) - \boldsymbol{r}(t)\big) - \frac{2}{t_f - t} \big(\dot{\boldsymbol{\rho}}(t_f) - \dot{\boldsymbol{r}}(t)\big) \\ &- \frac{6}{t_f - t} \dot{\boldsymbol{\rho}}(t_f) \end{aligned}$$

In order to avoid singularity at the time close to the final time, the acceleration trajectory should be set to zero when $|t - t_f|$ becomes sufficiently small.

B. Optimal Rendezvous Time

If the terminal time t_f is given, then $\boldsymbol{\rho}(t_f)$ and $\dot{\boldsymbol{\rho}}(t_f)$ can be computed from (18). However, the optimal terminal time, t_f^* remains to be found. The *optimal Hamiltonian* $\mathcal{H}^* = \mathcal{H}(\boldsymbol{x}^*, \boldsymbol{u}^*, \boldsymbol{\lambda})$ calculated at optimal point $\boldsymbol{u}^*$ and $\boldsymbol{x}^*$ must satisfy $\mathcal{H} = 0$, i.e.,

$$\mathcal{H}^*(t_f^*) = 1 - \kappa a_{\max}^2 - 2\kappa \|\boldsymbol{c}_2\|^2 + \boldsymbol{\lambda}_s^T \dot{\boldsymbol{s}} = 0, \tag{30}$$

Equation (30) gives the extra equation required to determine the optimal terminal time. We will show in the following analysis that $\boldsymbol{\lambda}_s^T \dot{\boldsymbol{s}}$ can be expressed as a function of t_f. The final values of the costate can be obtained from the end point constraint equation referred to as the *transversality* condition:

$$\boldsymbol{\lambda}(t_f) = \big(\boldsymbol{\psi}_{\boldsymbol{x}}^T \boldsymbol{\nu} + \phi_{\boldsymbol{x}}\big)_{\boldsymbol{x}_f} \tag{31}$$

where $\boldsymbol{\psi}_{\boldsymbol{x}}$ is shorthanded for $\partial \boldsymbol{\psi} / \partial \boldsymbol{x}$, $\phi_{\boldsymbol{x}}$ is similarly defined, and $\boldsymbol{\nu} = [\boldsymbol{\nu}_1^T \ \boldsymbol{\nu}_2^T]^T$ with $\boldsymbol{\nu}_1, \boldsymbol{\nu}_2 \in \mathbb{R}^3$. Using (21) and (22) in (31) yields

$$\begin{aligned} \boldsymbol{\lambda}_s(t_f) &= \frac{\partial \boldsymbol{\rho}^T}{\partial \boldsymbol{s}} \boldsymbol{\nu}_1 + \frac{\partial \dot{\boldsymbol{\rho}}^T}{\partial \boldsymbol{s}} \boldsymbol{\nu}_2 + \phi_{\boldsymbol{s}} \\ \phi_{\boldsymbol{r}} - \boldsymbol{\nu}_1 &= 2\kappa \boldsymbol{c}_1 \\ -\boldsymbol{\nu}_2 + -2\kappa \boldsymbol{c}_1 (t_f - t_o) - 2\kappa \boldsymbol{c}_2 \end{aligned} \tag{32}$$

in which all variables are calculated at the final time t_f. Now, equating right-hand sides of (27) and (32) will result

in a set of three equations with three unknowns $\boldsymbol{\nu}_1$, $\boldsymbol{\nu}_2$, and $\boldsymbol{\lambda}_s^T \dot{\boldsymbol{s}}$. Solving the set of equations gives the following useful identity

$$\boldsymbol{\lambda}_s^T \dot{\boldsymbol{s}} = (\phi_{\boldsymbol{r}} - 2\kappa \boldsymbol{c}_1)^T \dot{\boldsymbol{\rho}} + 2\kappa \big(\boldsymbol{c}_1(t_f - t_o) + \boldsymbol{c}_2\big)^T \ddot{\boldsymbol{\rho}} + \dot{\phi}, \quad (33)$$

in which $\ddot{\boldsymbol{\rho}}$ and $\dot{\phi}$ can be computed from

$$\ddot{\boldsymbol{\rho}} = \boldsymbol{A}(\boldsymbol{q})\Big(\boldsymbol{\omega} \times (\boldsymbol{\omega} \times \boldsymbol{\varrho}) + \boldsymbol{d}(\boldsymbol{\omega}) \times \boldsymbol{\varrho}\Big)$$

$$\dot{\phi} = \frac{1}{2} \phi_{\boldsymbol{r}}^T \boldsymbol{\Omega}(\boldsymbol{\omega}) \boldsymbol{q}$$

Finally, substituting (33) into (30) and using the optimal motion trajectories, we will arrive at

$$\begin{aligned} \mathcal{H}(t_f) =& 1 - \kappa a_{\max}^2 - 2\kappa \left\|\boldsymbol{c}_2\right\|^2 + \dot{\phi} + 2\kappa \boldsymbol{c}_2^T \ddot{\boldsymbol{\rho}} \\ &+ (\boldsymbol{c}_2^T \phi_{\boldsymbol{r}} - 2\kappa \boldsymbol{c}_1^T \boldsymbol{c}_2 + 2\kappa \ddot{\boldsymbol{\rho}}^T \boldsymbol{c}_1)(t_f - t_o) \\ &+ (0.5 \boldsymbol{c}_1^T \phi_{\boldsymbol{r}} - \kappa \|\boldsymbol{c}_1\|^2)(t_f - t_o)^2 = 0 \end{aligned} \quad (34)$$

The zero crossing solution, i.e., optimal rendezvous time, of the explicit equation (34) can obtained using a numerical method such as the Newton-Raphson (NR) method.

IV. Post-Grasping Trajectory Planning

After grasping of the uncontrolled drifting and tumbling space object by the manipulator, the manipulator should gently exert force and torque to the object for stopping its linear and angular motion; see Fig. 2(b). This section describes robot trajectory planning for fast dissipation of the angular and linear momentums of the grasped object subject to the constraint that the magnitude of the interaction force and torque between the manipulator's end-effector and the tumbling satellite remain below their pre-specified maximum values. We assume that *a priori* estimates of target mass, m, and the trace of its inertia tensor are available. Therefore, the absolute inertia can be computed from the estimations of the relative inertia by

$$I_{xx} = \frac{\mathrm{tr}(\boldsymbol{I}_c)}{b_x(\boldsymbol{\sigma})} \quad , I_{yy} = \frac{\mathrm{tr}(\boldsymbol{I}_c)}{b_y(\boldsymbol{\sigma})}, \quad I_{zz} = \frac{\mathrm{tr}(\boldsymbol{I}_c)}{b_z(\boldsymbol{\sigma})}$$

Denoting the linear and angular momentums of the target as $\boldsymbol{h} = \boldsymbol{I}_c \boldsymbol{\omega}$ and $\boldsymbol{p} = m\boldsymbol{v}$, we can write the dynamics of the target in the post-grasping phase

$$\dot{\boldsymbol{p}} + \boldsymbol{\omega} \times \boldsymbol{p} = \boldsymbol{f} \quad (35a)$$

$$\dot{\boldsymbol{h}} + \boldsymbol{\omega} \times \boldsymbol{h} = \boldsymbol{\tau} - \boldsymbol{\varrho} \times \boldsymbol{f}, \quad (35b)$$

where $\boldsymbol{f}$ and $\boldsymbol{\tau}$ are the force and torque exerted by the robot's end-effector to the target. The objective is to damp out the initial linear and angular momentums of the target right after grasping, i.e., $\boldsymbol{p}(0)$ and $\boldsymbol{h}(0)$, as quickly as possible subject to the the force and torque limits. That is, the torque and force trajectories should satisfy

$$\begin{aligned} &\|\boldsymbol{p}\| \to 0 \quad \text{and} \quad \|\boldsymbol{h}\| \to 0 \\ \text{s.t.:} \quad &\|\boldsymbol{f}\| \le f_{\max} \quad (36a) \\ &\|\boldsymbol{\tau}\| \le \tau_{\max} \quad (36b) \end{aligned}$$

Define positive function

$$V = \|\boldsymbol{p}\| + \|\boldsymbol{h}\| \quad (37)$$

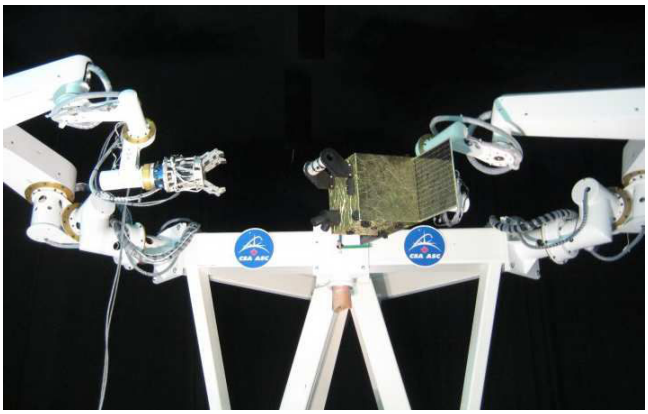

Fig. 2. The experimental setup

Then, the time-derivative of V along trajectories of (35) yields

$$\begin{aligned} \dot{V} &= \frac{\boldsymbol{p}^T \dot{\boldsymbol{p}}}{\|\boldsymbol{p}\|} + \frac{\boldsymbol{h}^T \dot{\boldsymbol{h}}}{\|\boldsymbol{h}\|} \\ &= \frac{-\boldsymbol{p}^T \boldsymbol{\omega} \times \boldsymbol{p} + \boldsymbol{p}^T \boldsymbol{f}}{\|\boldsymbol{p}\|} + \frac{-\boldsymbol{h}^T \boldsymbol{\omega} \times \boldsymbol{h} + \boldsymbol{h}^T \boldsymbol{\tau} - \boldsymbol{h}^T \boldsymbol{\varrho} \times \boldsymbol{h}}{\|\boldsymbol{h}\|} \\ &= (\boldsymbol{e}_p - \boldsymbol{\varrho} \times \boldsymbol{e}_h)^T \boldsymbol{f} + \boldsymbol{e}_h^T \boldsymbol{\tau} \end{aligned} \quad (38)$$

where

$$\boldsymbol{e}_p = \frac{\boldsymbol{p}}{\|\boldsymbol{p}\|} \quad \text{and} \quad \boldsymbol{e}_h = \frac{\boldsymbol{h}}{\|\boldsymbol{h}\|} \quad (39)$$

are unit vectors in the directions of the linear and angular momentum vectors. It is clear form (38) that in order to dump the linear and angular momentums as quickly as possible given the force/momnt limits (36a), the force and torque should take the forms

$$\boldsymbol{f} = -\frac{\boldsymbol{e}_p - \boldsymbol{\varrho} \times \boldsymbol{e}_h}{\|\boldsymbol{e}_p - \boldsymbol{\varrho} \times \boldsymbol{e}_h\|} f_{\max} \quad (40a)$$

$$\boldsymbol{\tau} = -\boldsymbol{e}_h \tau_{\max} \quad (40b)$$

Finally, substituting (40) into (35), we arrive at the Cartesian motion trajectories

$$\begin{aligned} \dot{\boldsymbol{\omega}}^* &= \boldsymbol{d}(\boldsymbol{\omega}) - \frac{\boldsymbol{\omega}}{\|\boldsymbol{h}\|} \tau_{\max} \\ \dot{\boldsymbol{v}}^* &= -\boldsymbol{\omega} \times \boldsymbol{v} - \frac{\boldsymbol{e}_p - \boldsymbol{\varrho} \times \boldsymbol{e}_h}{m\|\boldsymbol{e}_p - \boldsymbol{\varrho} \times \boldsymbol{e}_h\|} f_{\max} \\ \ddot{\boldsymbol{r}}^* &= \boldsymbol{A}(\boldsymbol{q})\big(\dot{\boldsymbol{v}}^* + \dot{\boldsymbol{\omega}}^* \times \boldsymbol{\varrho} + \boldsymbol{\omega} \times (\boldsymbol{\omega} \times \boldsymbol{\varrho})\big) \end{aligned}$$

In order to avoid chartering when the magnitude of the linear or angular momentum is small, the unit vectors can be redefined as

$$\boldsymbol{e}_h = \begin{cases} \frac{\boldsymbol{h}}{\|\boldsymbol{h}\|} & \text{if} \quad \|\boldsymbol{h}\| \le \epsilon \\ 0 & \text{otherwise} \end{cases}$$

and $\boldsymbol{e}_p$ is similarly defined.

V. End-to-End Validation by Experiment and Simulation

This section reports end-to-end validation of the performance of the robot motion guidance method to intercept

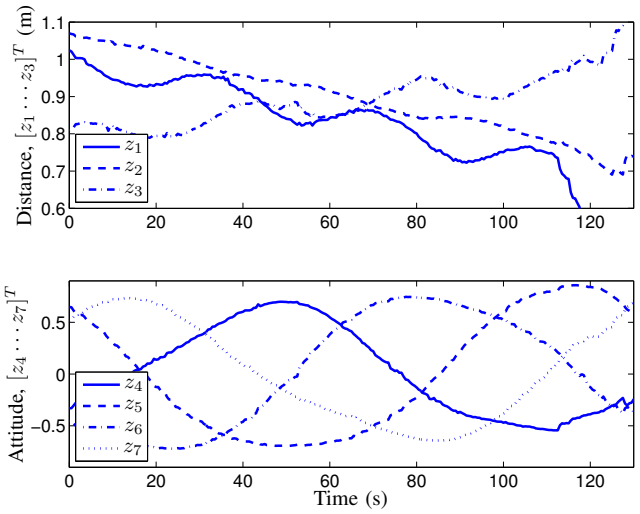

Fig. 3. Target pose measurements obtained from LCS.

and then stabilize a tumbling/drifting free-floater through combination of experiment and simulation. The learning phase and pre-grasping phase part of trajectory planning is demonstrated by experimental results. However, the post-grasping phase part is simulated based on initial values obtained from snapshot of the terminal states of the experimental system right at the time of interception. Fig. 2 illustrates the experimental setup with two manipulator arms. One arm is employed to move the mockup of a target satellite according to the motion of a tumbling/drifting free-floater. The other arm is used to autonomously approach the mockup and capture its grapple fixture. Neptec's Laser Camera System (LCS) [19] is used to obtain the range data at a rate of 2 Hz. The target pose is estimated by comparing the range data obtained from the LCS against the CAD model of the mockup using the Iterative Closest Point (ICP) algorithm [20].

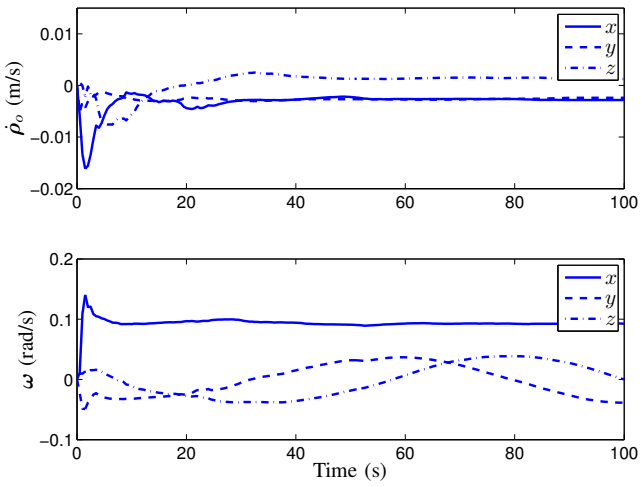

Fig. 4. Estimated drift velocity and angular velocity of the target.

The robotic arm to which the satellite mockup is attached is controlled so as to precisely mimic the free-floating

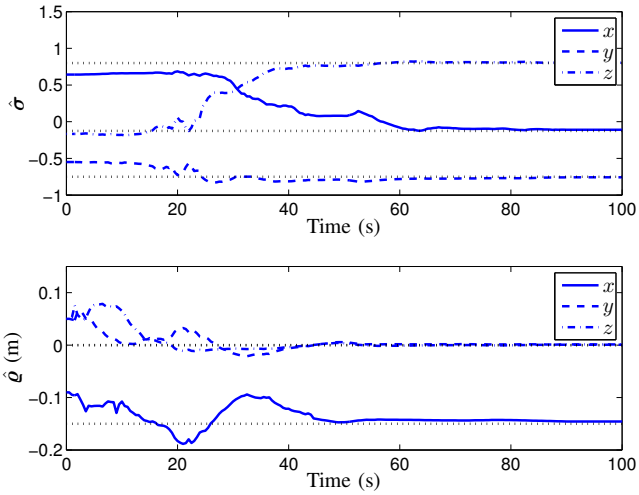

Fig. 5. Convergence of the estimated dynamics parameters of the target to their true values (depicted by dotted-lines).

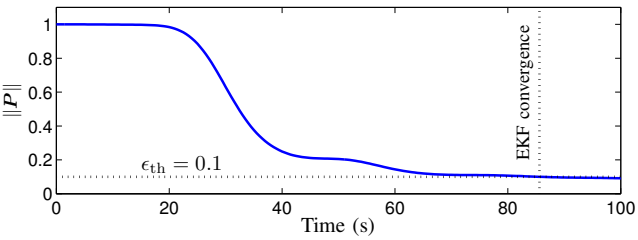

Fig. 6. Detecting the estimator convergence from the norm of the state covariance matrix.

dynamics motion of a target satellite. The moment of inertia values of the target satellite are selected as $I_{xx} = 16$ kgm^2, $I_{yy} = 32$ kgm^2, $I_{zz} = 20$ kgm^2, $m = 400$ kg, and the location of CM is $\boldsymbol{\varrho} = [-0.15 \ 0 \ 0]^T$ m. These values are used to determine the manipulator-driven motion of the target as free-floating object with initial drift velocity $\dot{\boldsymbol{\rho}}_o(0) = [-3 \ \ -2 \ 1.5]$ mm/s and initial angular velocity $\boldsymbol{\omega}(0) = [0.09 \ -0.04 \ 0.03]$ rad/s. The maximum acceleration and the contact torque/force are specified as

$$\text{constraints:} \begin{cases} a_{\max} = 0.02 \text{ m/s}^2 \\ f_{\max} = 0.1 \text{ N} \\ \tau_{\max} = 0.1 \text{ Nm} \end{cases}$$

All dynamics parameters with the exception of the mass the trace of the inertial tensor, $\text{tr}(\boldsymbol{I}_c) = 68$ kgm^2, are assumed to be unknown to the trajectory planner.

The time-history of the position and orientation of the mockup satellite obtained from ICP algorithm are shown in Fig. 3. Apparently, the vision system is obstructed by the robotic arm during its final approach at time $t = 112$ s. and thereafter the visual pose measurements are incorrect. During the learning phase, the EKF estimator receives these noisy measurements and subsequently estimates the sets of inertial parameters plus the linear and angular velocities of the tumbling satellite. Figs. 4 and 5 show the trajectories of the estimated velocities and the inertial parameters, respectively. The

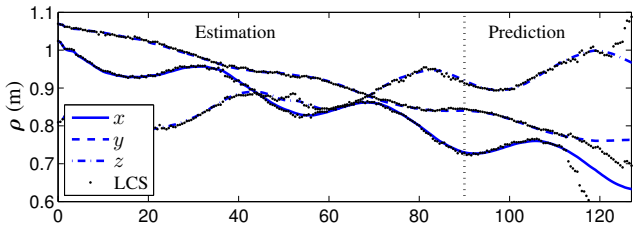

Fig. 7. Estimations and predictions of the grapple-fixture position.

motion planner automatically generates robot trajectory once the EKF estimator converges. To this end, the convergence is when the Euclidean norm of the state covariance matrix drops below a threshold ϵ_{th}, i.e., $\|\boldsymbol{P}_k\| \leq \epsilon_{\text{th}}$. It is apparent from the time-history of the covariance matrix norm in Fig. 6 that at time $t = 85$ s, the trajectory reaches the prescribed threshold $\epsilon_{\text{th}} = 0.1$ indicating the filter convergence. The initial time, however, is set to $t_o = 90$ s, leaving a conformable margin of 5 s to accommodate the computation time needed for path planning. Trajectories of the predicted position of the grapple fixture calculated from the latest estimation of the motion states and parameters of the target are shown in Fig. 7. A comparison of the trajectories of the visual measurements and those of the predicted position in Fig. 7a reveals that the visual measurements are not reliable at the final stages of the robot approach after time $t = 112$ s due to obstruction of the vision system by the approaching arm. The optimal rendezvous time, t_f, is obtained from solving the Hamiltonian as function of t_f in (34) using the predicted motion trajectories. The zero-crossing of the Hamiltonian numerically is found (using the Newton-Raphson method) to be $t_f = 126.5$ s as illustrated in Fig. 8. Trajectories of the robot's end-effector and the satellite grapple fixture in the pre- and post-grasping phases are shown in Fig. 9. It is evident that the robot intercepts the handle at the designated time $t = 126.5$ s and then the motion stopped at $t = 144$ s. Robotic capturing of the target satellite also requires that the robot end-effector is properly aligned with the target at the time of rendezvous. By virtue of (2), one can estimate the target angular acceleration from the estimated angular velocity and parameters according to $\hat{\dot{\boldsymbol{\omega}}} = \boldsymbol{d}(\hat{\boldsymbol{\omega}}, \hat{\boldsymbol{\sigma}})$. Consequently, $\hat{\boldsymbol{q}}$, $\hat{\boldsymbol{\omega}}$, and $\hat{\dot{\boldsymbol{\omega}}}$ constitute the desired orientation trajectories of the robot. Fig. 10 demonstrates that the robot end-effector is able to track the target attitude few seconds after the initial time. Figs. 11 and 12, respectively, show trajectories of the linear and angular velocities of the end-effector versus those of the grapple fixture before and after the interception. It is clear from the plot that the end-effector has reached the grapple fixture with the same velocity and the time of the rendezvous at the time $t = 126.5$ s and then the velocities completely decayed to zero at the time $t = 144$ s.

VI. Conclusion

Visual guidance of a robotic manipulator to first intercept and then stabilize a drifting and tumbling space object with uncertain dynamics has been presented. A Kalman filter was

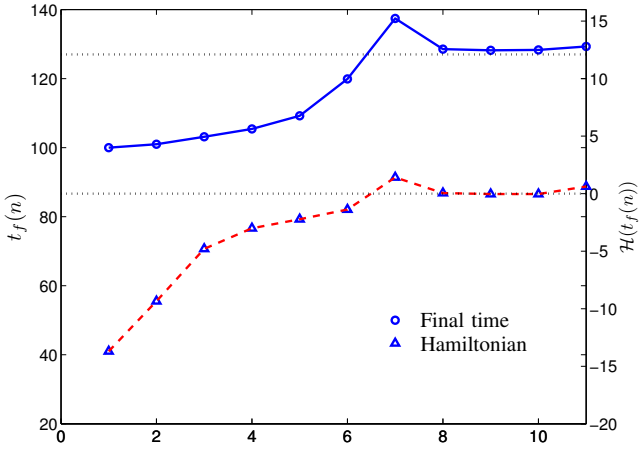

Fig. 8. NR iterations to find the zero crossing of the Hamiltonian function.

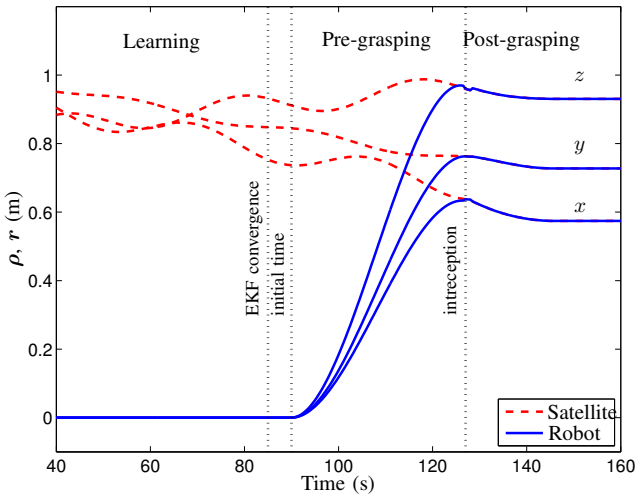

Fig. 9. Position trajectories of the satellite's handle and the robot's hand in the learning, pre-grasping, and post-grasping phases.

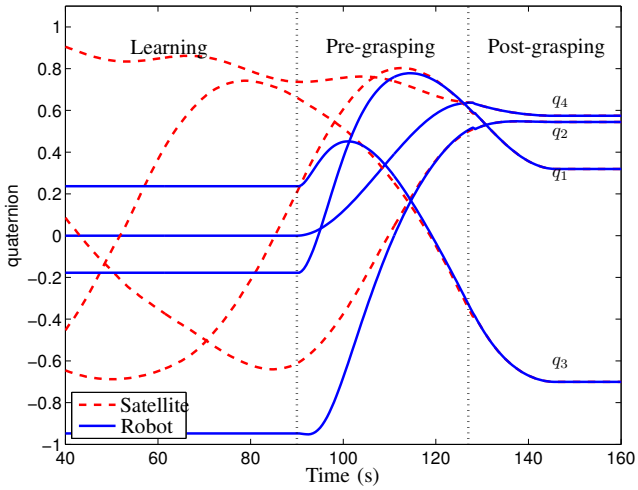

Fig. 10. Oreintation trajectories of the satellite's handle and the robot's hand in the learning, pre-grasping, and post-grasping phases.

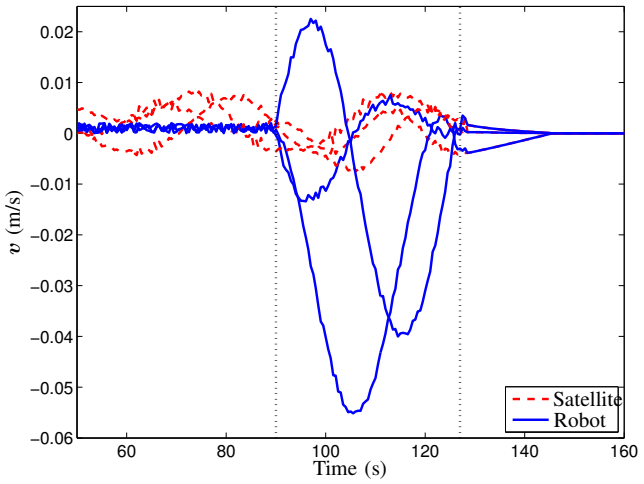

Fig. 11. Linear velocities of the robot and stallite before and after grasping.

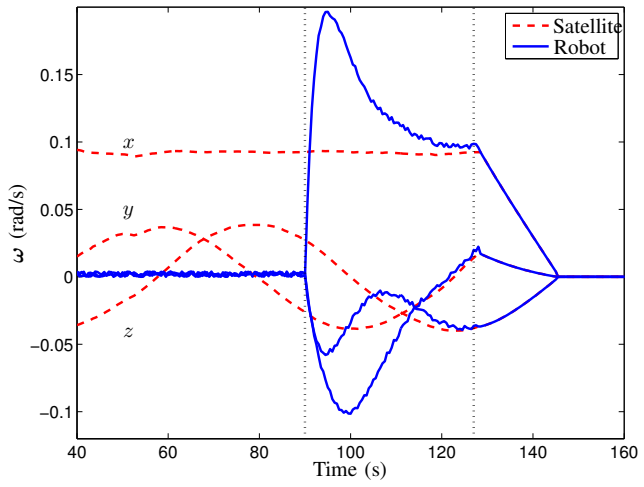

Fig. 12. Angular velocities of the robot and stallite before and after grasping.

used to estimate the motion states and a set of dynamics parameters of the target based on noisy pose measurements of a laser camera system. The estimations of the states and parameters were used by the guidance scheme to optimally plan the trajectory of the robot's end-effector in the pre- and post-grasping phases. For the pre-grasping phase, an optimal trajectory was designed for intercepting a grapple fixture on the target minimizing a cost function as a weighted linear sum of travel time, distance, and cosine of a line-of-sight angle subject to acceleration limit. In the post-grasping phase, another optimal trajectory ensures that the drafting and tumbling object is brought to state of rest as quickly as possible subject to force and torque limits. Finally, the performance of the proposed autonomous guidance method for robotic capture and stabilization of a tumbling satellite was demonstrated by combination of experimental and simulation results.

ACKNOWLEDGMENT

This work was supported by Canadian Space Agency and Natural Sciences and Engineering Research Council of Canada (NSERC) under grant RGPIN/288255-2011.

REFERENCES

[1] D. Whelan, E. Adler, S. Wilson, and G. Roesler, "Darpa orbital express program: effecting a revolution in space-based systems," in *Small Payloads in Space*, vol. 136, Nov. 2000, pp. 48–56.

[2] S. Kawamoto, S. Nishida, and S. Kibe, "Research on a space debris removal system," *NAL Res Prog (National Aerospace Lab. Japan)*, vol. 2002/2003, pp. 84–87, 2003.

[3] *On-Orbit Satellite Servicing Study, Project Report*, National Aeronautics and Space Administration, Goddard Space Flight Center, 2010.

[4] G. Brachet, "Long-term sustainability of outer space activities," Committee on the Peaceful Uses of Outer Space (UNCOPUOS), Vienna, Tech. Rep., 8-19 February 2010.

[5] D. Kessler, R. Reynold, and P. Ans-Meador, "TM 100-471 orbital debris environment for spacecraft designed to operate in low earth orbit," NASA JSC,, Houston, TX, Tech. Rep., 1989.

[6] J.-C. Liou, N. Johnson, and N. Hill, "Controlling the growth of future LEO debris populations with active debris removal," *Acta Astronautica*, vol. 66, no. 5-6, pp. 648–653, March-April 2009.

[7] B. Barbee, S. Alfano, E. Pinon, K. Gold, and D. Gaylor, "Design of spacecraft missions to remove multiple orbital debris objects," in *Aerospace Conference, 2011 IEEE*, march 2011, pp. 1–14.

[8] N. Inaba and M. Oda, "Autonomous satellite capture by a space robot: world first on-orbit experiment on a japanese robot satellite ets-vii," in *Robotics and Automation, 2000. Proceedings. ICRA '00. IEEE International Conference on*, 2000.

[9] K. Yoshida, "Engineering test satellite VII flight experiment for space robot dynamics and control: Theories on laboratory test beds ten years ago, now in orbit," *The Int. Journal of Robortics Research*, vol. 22, no. 5, pp. 321–335, 2003.

[10] G. Hirzinger, K. Landzettel, B. Brunner, M. Fisher, C. Preusche, D. Reintsema, A. Albu-Schaffer, G. Schreiber, and B.-M.Steinmetz, "DLR's robotics technologies for on-orbit servicing," *Advanced Robotics*, vol. 18, no. 2, pp. 139–174, 2004.

[11] Z. Vafa and S. Dubowsky, "On the dynamics of manipulators in space using the virtual manipulator approach," in *IEEE Int. Conf. on Robotics & Automation*, Raleigh, NC, 1987, pp. 579–585.

[12] E. Papadopoulos and S. Dubowsky, "On the nature of control algorithms for space manipulators," in *IEEE Int. Conf. on Robotics & Automation*, 1990, pp. 1102–1108.

[13] S. Matsumoto, Y. Ohkami, Y. Wakabayashi, M. Oda, and H. Uemo, "Satellite capturing strategy using agile orbital servicing vehicle, hyper osv," in *IEEE Int. Conf. on Robotics & Automation*, Washington DC, May 2002, pp. 2309–2314.

[14] E. A. Croft, R. G. Fenton, and B. Benhabib, "Optimal rendezvous-point selection for robotic inteception of moving objects," *IEEE Trans. on Systems, Man, and Cybernetics*, vol. 28, no. 2, pp. 192–204, Apr. 1998.

[15] M. Mehrandezh, N. M. Sela, R. G. Fenton, and B. Benhabib, "Robotic interception of moving objects using an augmented ideal proportional navigation guidance technique," *IEEE Trans. on Systems, Man, and Cybernetics*, vol. 30, no. 3, pp. 238–250, May 2000.

[16] C. Li, B. Liang, and W. Xu, "Autonomous trajectory planning of free-floating robot for capturing space target," in *Intelligent Robots and Systems, 2006 IEEE/RSJ International Conference on*, 2006, pp. 1008–1013.

[17] F. Aghili, "A prediction and motion-planning scheme for visually guided robotic capturing of free-floating tumbling objects with uncertain dynamics," *IEEE Trans. on Robotics*, vol. 28, no. 3, pp. 634–649, June 2012.

[18] B. D. O. Anderson and J. B. Moore, *Optimal Control*. Englewood Cliffs, NJ: Prince Hall, 1990.

[19] C. Samson, C. English, A. Deslauriers, I. Christie, F. Blais, and F. Ferrie, "Neptec 3D laser camera system: From space mission STS-105 to terrestrial applications," *Canadian Aeronautics and Space Journal*, vol. 50, no. 2, pp. 115–123, 2004.

[20] F. Aghili, M. Kuryllo, G. Okouneva, and C. English, "Fault-tolerant position/attitude estimation of free-floating space objects using a laser range sensor," *IEEE Sensors Journal*, vol. 11, no. 1, pp. 176–185, Jan. 2011.